Naval Research Laboratory

Washington, DC 20375-5320

NRL/MR/5650--10-9275

Radio-Frequency Down-Conversion via Sampled Analog Optical Links

JASON D. MCKINNEY
VINCENT J. URICK

Photonics Technology Branch
Optical Sciences Division

August 9, 2010

Approved for public release; distribution is unlimited.

REPORT DOCUMENTATION PAGE

Form Approved
OMB No. 0704-0188

Public reporting burden for this collection of information is estimated to average 1 hour per response, including the time for reviewing instructions, searching existing data sources, gathering and maintaining the data needed, and completing and reviewing this collection of information. Send comments regarding this burden estimate or any other aspect of this collection of information, including suggestions for reducing this burden to Department of Defense, Washington Headquarters Services, Directorate for Information Operations and Reports (0704-0188), 1215 Jefferson Davis Highway, Suite 1204, Arlington, VA 22202-4302. Respondents should be aware that notwithstanding any other provision of law, no person shall be subject to any penalty for failing to comply with a collection of information if it does not display a currently valid OMB control number. **PLEASE DO NOT RETURN YOUR FORM TO THE ABOVE ADDRESS.**

1. REPORT DATE *(DD-MM-YYYY)*	**2. REPORT TYPE**	**3. DATES COVERED** *(From - To)*
08-09-2010	Memorandum Report	May 1, 2010 - July 31, 2010

4. TITLE AND SUBTITLE

Radio-Frequency Down-Conversion via Sampled Analog Optical Links

5a. CONTRACT NUMBER

5b. GRANT NUMBER

5c. PROGRAM ELEMENT NUMBER
62271N

6. AUTHOR(S)

Jason D. McKinney and Vincent J. Urick

5d. PROJECT NUMBER

5e. TASK NUMBER
EW-271-003

5f. WORK UNIT NUMBER
6308

7. PERFORMING ORGANIZATION NAME(S) AND ADDRESS(ES)

Naval Research Laboratory, Code 5650
4555 Overlook Avenue, SW
Washington, DC 20375-5320

8. PERFORMING ORGANIZATION REPORT NUMBER

NRL/MR/5650--10-9275

9. SPONSORING / MONITORING AGENCY NAME(S) AND ADDRESS(ES)

Office of Naval Research
875 North Randolph Street
Arlington, VA 22203-1995

10. SPONSOR / MONITOR'S ACRONYM(S)
ONR

11. SPONSOR / MONITOR'S REPORT NUMBER(S)

12. DISTRIBUTION / AVAILABILITY STATEMENT

Approved for public release; distribution is unlimited.

13. SUPPLEMENTARY NOTES

14. ABSTRACT

In this work we derive and experimentally verify the radio-frequency performance of a down-converter employing a sampled analog optical link. We show that the down-converter operation is well described by conventional analog optical link theory, with additional impact from the sampling optical pulse shape. We also demonstrate that the required photodiode performance is determined only by the sampling rate — not the highest frequency of interest. We verify our analysis with an experimental demonstration of down-conversion of radio-frequency signals in the 1–10 GHz range using a 1-GHz sampled analog optical link.

15. SUBJECT TERMS
Analog photonics Electronic support measures
Built-in-test

16. SECURITY CLASSIFICATION OF:			**17. LIMITATION OF ABSTRACT**	**18. NUMBER OF PAGES**	**19a. NAME OF RESPONSIBLE PERSON**
					Jason D. McKinney
a. REPORT	**b. ABSTRACT**	**c. THIS PAGE**	UL	17	**19b. TELEPHONE NUMBER** *(include area code)*
Unclassified	Unclassified	Unclassified			(202) 404-4207

Standard Form 298 (Rev. 8-98)
Prescribed by ANSI Std. Z39.18

CONTENTS

I EXECUTIVE SUMMARY

In this work we derive and experimentally verify the radio-frequency performance of a down-converter employing a sampled analog optical link. We show that the down-converter operation is well-described by conventional analog optical link theory, with additional impact from the sampling optical pulse shape. We also demonstrate that the required photodiode performance is determined only by the sampling rate - not the highest frequency of interest. We verify our analysis with an experimental demonstration of down-conversion of radio-frequency signals in the 1–10 GHz range using a 1-GHz sampled analog optical link.

II INTRODUCTION

Over the past 30 years, there has been significant interest in accomplishing analog-to-digital conversion (ADC) via photonic, or photonically-enabled architectures [1]. Many of the arguments for using photonics for ADC applications are the same as for using photonics for analog radio-frequency (RF) signal transmission (microwave photonics) [2]. Optics possess bandwidth far beyond electronics, offers a measure of immunity from electromagnetic interference, and enables exceedingly low loss transmission over very large distances. These properties make photonic architectures appealing for a variety of analog and digital applications.

While there have been a variety of photonic ADCs demonstrated (see [1]), of particular interest are the class of photonically-enabled ADCs which utilize short optical pulses to sample an electronic signal [3, 4] via an electrooptic modulator [5, 6, 7, 8, 9, 10]. Because the optical power transmission of an electro-optic modulator (typically an integrated lithium-niobate Mach-Zehnder modulator, or MZM) is proportional to the applied radio-frequency (RF) voltage, the pulse energy out of the modulator represents the sampled voltage at a particular instant in time. The output pulses are then detected with a photodetector, the output of which is filtered, potentially further processed, and electronically quantized with a high-quality electronic ADC. While all of these architectures [5, 6, 7, 8, 9] employ an externally-modulated analog optical link, only recently has the RF performance of a sampled analog optical link (the first operation in a photonically sampled ADC) been described [11] using conventional analog link theory [12, 13].

Here, we describe the use of a sampled analog link to achieve down-conversion (spectral-folding, or aliasing) of RF signals for wideband electronic warfare applications. We note, this concept has been utilized in optically sampled ADCs [14, 10] as well as time-interleaved hybrid ADCs [7, 8]. Here, however, we provide the first analog description of the down-conversion operation to the our knowledge. Note, the scope of this report is limited to the RF performance of the down-converting sampled link – we do not discuss quantization of the sampled signal. For a thorough discussion of quantization in photonically-sampled systems, the reader should consult [1] and references therein. The remainder of this report is structured as follows: In Section III we provide a brief theoretical description of the sampled link and mathematically describe the down-conversion operation. We additionally derive the RF gain of the sampled link operating in a down-converting mode, provide the relevant RF performance metrics, and discuss the impact of the optical pulsewidth on the wideband performance of the system. Section IV details a proof-of-concept experiment employing a 1-GHz sampled link. Here we experimentally measure the RF gain and linearity across several Nyquist bands to validate the theoretical derivation in Section III. This section also demonstrates the effects of the finite optical pulsewidth and photodiode performance on the down-conversion operation. In Section V we summarize the work and point to several directions for future research.

III THEORY OF DOWNCONVERSION VIA A SAMPLED OPTICAL LINK

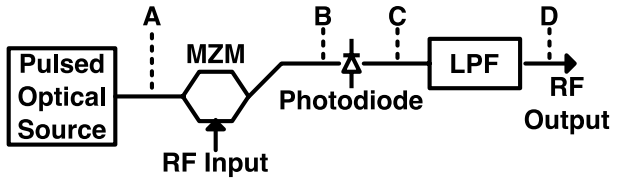

Fig. 1: Sampled optical link. MZM: Mach-Zehnder modulator, LPF: low-pass filter

In a quadrature-biased IMDD link employing a dual-output MZM, the time-domain output photocurrents

Manuscript approved June 14, 2010.

(in reference to Fig. 1, these are measured at point **C**) may generally be written as [11]

$$i_{1,2}(t) = \frac{1}{2} p_{\text{opt}}(t) \left\{1 \pm \sin[v_{\text{in}}(t) * h_{\text{mzm}}(t)]\right\} * h_{\text{pd}}(t)\,. \tag{1}$$

Here, $p_{\text{opt}}(t)$ is the intensity (power) envelope of the optical carrier as measured at the input of the MZM (point **A** in Fig. 1), $v_{\text{in}}(t)$ is the input RF voltage, $h_{\text{mzm}}(t)$ is the impulse response of the Mach-Zehnder modulator, and $h_{\text{pd}}(t)$ is the impulse response of the photodiode. The impulse response of the MZM is related to the more commonly used frequency-dependent halfwave voltage by the relation

$$\begin{aligned} h_{\text{mzm}}(t) &= \frac{1}{2\pi} \int_{-\infty}^{\infty} d\omega \, \frac{\pi}{V_\pi(\omega)} \exp(j\omega t) \\ &= \mathcal{F}^{-1}\left\{\frac{\pi}{V_\pi(\omega)}\right\}. \end{aligned} \tag{2}$$

The photodiode impulse response is normalized such that

$$\int_{-\infty}^{\infty} dt \, h_{\text{pd}}(t) = \alpha(\omega = 0)\,, \tag{3}$$

where $\alpha(\omega = 0)$ (A/W) is the DC responsivity of the photodiode. Although only one output is shown in Fig. 1, the subscripts (1, 2) designate the two separate RF outputs from the link, each derived from one arm of the MZM. Note, the complementary nature of the modulation between the outputs allows the use of balanced detection for noise rejection and increased link gain. When small-signal conditions apply

$$\left|v_{\text{in}}(t) * h_{\text{mzm}}(t)\right|_{\text{max}} \ll 1 \text{ (rad)} \tag{4}$$

we may approximate the sine by its argument which yields a linear relation between the input voltage and output photocurrents

$$i_{1,2}(t) = \frac{1}{2} p_{\text{opt}}(t) \left[1 \pm v_{\text{in}}(t) * h_{\text{mzm}}(t)\right] * h_{\text{pd}}(t)\,. \tag{5}$$

The complex photocurrent spectra of the link output are given by the Fourier transform of (5)

$$I_{1,2}(\omega) = \frac{P_{\text{opt}}(\omega)}{2} H_{\text{pd}}(\omega) \pm \left[\frac{\pi}{2} P_{\text{opt}}(\omega) * \frac{V_{\text{in}}(\omega)}{V_\pi(\omega)}\right] H_{\text{pd}}(\omega)\,. \tag{6}$$

Here, $P_{\text{opt}}(\omega)$ is the Fourier transform of the temporal optical intensity profile and $H_{\text{pd}}(\omega)$ is the electrical frequency response of the photodiode. The first term in (6) represents the spectral contribution arising solely from photodetection of the optical carrier. The spectrum of the temporal intensity $P_{\text{opt}}(\omega)$ includes intensity noise quantities arising from the optical source (e.g. laser intensity noise, amplified spontaneous emission from an optical amplifier). Note, this contribution to the RF spectrum is common-mode to both outputs and, therefore, may be suppressed via balanced detection. The second term gives the photocurrent spectrum resulting from the applied RF modulation $V_{\text{in}}(\omega)$. Thus far, we have not specified the temporal shape of either the intensity of the optical carrier or the input RF voltage; therefore (5) and (6) are general expressions for the output time-domain photocurrent and complex RF power spectra, respectively, for a dual-output MZM-based intensity-modulated direct-detection (IMDD) link.

In the sampled link architecture, the optical carrier is periodically pulsed – the temporal intensity profile of the optical source (point **A** in Fig. 1) is, therefore, composed of a train of optical pulses with a pulse-period of T seconds (repetition-rate $f_{\text{rep}} = 1/T$). Within a single period the intensity envelope (pulse shape) is given by the function $\tilde{p}_{\text{opt}}(t)$ and the pulse train is expressed as

$$p_{\text{opt}}(t) = \tilde{p}_{\text{opt}}(t) * \sum_{n=-\infty}^{\infty} \delta\left(t - nT\right), \tag{7}$$

where δ is the Dirac delta-function. The periodic temporal nature of the optical carrier gives rise to a comb spectrum

$$\begin{aligned} P_{\text{opt}}(\omega) &= \tilde{P}_{\text{opt}}(\omega) \times \sum_{n=-\infty}^{\infty} \delta\left(\omega - n2\pi f_{\text{rep}}\right) \\ &= \sum_{n=-\infty}^{\infty} P_n \delta\left(\omega - n2\pi f_{\text{rep}}\right) \end{aligned} \tag{8}$$

where $\tilde{P}_{\text{opt}}(\omega)$ is the Fourier transform of the intensity envelope of a single pulse [$\tilde{p}_{\text{opt}}(t)$] in the optical pulse train and $P_n = \tilde{P}_{\text{opt}}\big(\omega = n2\pi f_{\text{rep}}\big)$ is the amplitude of the n-th order comb line. Inserting (8) into (6) the complex RF spectra may be written as

$$I_{1,2}(\omega) = \frac{1}{2} H_{\text{pd}}(\omega) \sum_{n=-\infty}^{\infty} P_n \delta\left(\omega - n2\pi f_{\text{rep}}\right) \pm \left[\frac{\pi}{2} \sum_{n=-\infty}^{\infty} P_n V'_{\text{in}}\big(\omega - n2\pi f_{\text{rep}}\big)\right] H_{\text{pd}}(\omega), \tag{9}$$

where

$$V'_{\text{in}}(\omega) = \frac{V_{\text{in}}(\omega)}{V_\pi(\omega)}. \tag{10}$$

From (9) we see the scaled input spectrum is replicated at integer multiples of the sampling rate f_{rep} as is expected for a sampled system.

When the photodiode output is passed through a low-pass filter with passband $H_{\text{lp}}(\omega)$ (cutoff frequency $\omega_{\text{lp}} = 2\pi f_{\text{rep}}/2$) it is readily seen that, for each index n, frequencies within the range of $2\omega_{\text{lp}} = 2\pi f_{\text{rep}}$ about the n-th comb-line

$$2\pi f_{\text{rep}}\left(n - \frac{1}{2}\right) < \omega < 2\pi f_{\text{rep}}\left(n + \frac{1}{2}\right) \tag{11}$$

will be folded (aliased) into the first Nyquist band ($m = 1$, $|\omega| < 2\pi f_{\text{rep}}/2$). Note, the Nyquist bands are defined as frequency bins bounded by integer multiples of one-half the sample rate (e.g., the $m = 1$ band corresponds to $0 \leq |f| < f_{\text{rep}}/2$, the $m = 2$ band corresponds to $f_{\text{rep}}/2 \leq |f| < f_{\text{rep}}$, etc). For a load resistance of R_{o} the RF power measured in the first Nyquist band is then expressed as [$P_{\text{rf}}(\omega) = 1/2I^2(\omega)R_{\text{o}}$]

$$P_{1,2}(\omega) = \frac{1}{2}\pi^2 \left| \sum_{n=-\infty}^{\infty} \frac{P_n}{2} V'_{\text{in}}\big(\omega - n2\pi f_{\text{rep}}\big) \right|^2 \left|H_{\text{pd}}(\omega)\right|^2 \left|H_{\text{lp}}(\omega)\right|^2 R_{\text{o}}. \tag{12}$$

Inserting (10) into (12), normalizing the n-th comb line amplitude to total the average optical power (P_{avg}) and using the fact that the photodiode response is normalized to the DC responsivity, the output RF power may be written as

$$P_{1,2}(\omega) = \frac{1}{2}\pi^2 I_{\text{avg}}^2 \left| \sum_{n=-\infty}^{\infty} \left(\frac{P_n}{P_{\text{avg}}}\right) \frac{V_{\text{in}}\big(\omega - n2\pi f_{\text{rep}}\big)}{V_\pi^2(\omega)} \right|^2 \left|H_{\text{pd}}(\omega)\right|^2 \left|H_{\text{lp}}(\omega)\right|^2 R_{\text{o}}, \tag{13}$$

where $I_{\text{avg}} = \alpha(\omega = 0)\, P_{\text{avg}}/2$ is the average photocurrent from a single diode.

When the input signal is known to fall within a particular Nyquist band (e.g., when a tunable pre-select filter is utilized) the summation in (13) only contains a single spectrum and the output power may be written as

$$P_{1,2}(\omega) = \frac{1}{2}\pi^2 \frac{I_{\text{avg}}^2}{V_\pi^2(\omega)} \left|\frac{P_n}{P_{\text{avg}}}\right|^2 |V_{\text{in}}(\omega)|^2 \left|H_{\text{pd}}(\omega)\right|^2 \left|H_{\text{lp}}(\omega)\right|^2 R_{\text{o}}. \tag{14}$$

Given the input power to the link at frequency ω is $P_{\text{in}} = 1/2\,|V_{\text{in}}(\omega)|^2 / R_{\text{i}}$ (where R_{i} is the input resistance of the modulator) the RF gain of the sampled link is given by (w/o considering photodiode impedance matching)

$$G_{1,2}(\omega) = \left|\frac{P_n}{P_{\text{avg}}}\right|^2 \left[\pi \frac{I_{\text{avg}}}{V_\pi(\omega)}\right]^2 \left|H_{\text{pd}}(\omega)\right|^2 \left|H_{\text{lp}}(\omega)\right|^2 R_{\text{i}} R_{\text{o}}. \tag{15}$$

Here, we see the gain of the sampled link in the higher Nyquist bands is equal to that in the first band [11], weighted by the square of the normalized power of the n-th optical comb line. Several other important aspects of the system are also apparent from (15). In particular, we see the gain uniformity (with respect to band order) improves with shorter sampling pulses [$\left|P_n/P_{\text{avg}}\right| \sim$ constant for larger n as the bandwidth increases]. Similar pulsewidth dependence has been documented in optically-sampled ADCs [14]. Because the down conversion operation occurs in the optical domain, we also see that a low-frequency photodiode (bandwidth $\sim f_{\text{rep}}/2$) may be utilized, regardless of the highest frequency signal to be sampled (only the response in the first Nyquist band is relevant).

It has been shown that the nonlinearity of the sampled link architecture is equivalent to that of a conventional analog optical link, in the absence of significant photodiode nonlinearity [11]. For brevity, we simply state that the the link linearity is limited by the third-order distortion introduced by the MZM and the two-tone output third-order intercept point for a single sampled link (w/o impedance-matched photodiodes) is given by

$$\text{OIP}_3 = 4 I_{\text{avg}}^2 R_{\text{o}} = \left(\frac{4}{\pi^2}\frac{V_\pi^2}{R_{\text{i}}}\right) \times G. \tag{16}$$

Here, the quantity in parenthesis is the input third-order intercept point and G is the RF gain of the link. While the noise floor (and, hence, noise figure and spurious-free dynamic range) may also be theoretically calculated for a link which does not utilize optical amplifiers, the use of an EDFA in this work precludes such analytic solutions. Therefore, we will treat the noise floor as a measured quantity and use the general expressions for noise factor

$$\text{nf} = \frac{1}{G}\frac{N_{\text{out}}}{k\text{T}} \tag{17}$$

and third-order-limited spur-free dynamic range

$$\text{SFDR} = \left(\frac{\text{OIP}_3}{N_{\text{out}}}\right)^{2/3}. \tag{18}$$

Above, N_{out} is the measured noise power spectral density (PSD) at the link output, k is Boltzmann's constant, and $T = 290$ K. We will now discuss one implementation of the down-converting sampled link and provide experimental data supporting the preceding analysis.

IV EXPERIMENT

Sampled Link Architecture and Down-Conversion

To demonstrate down-conversion via a sampled photonic link, we constructed the link shown schematically in Figure 2. The pulsed optical source is composed of a $\sim$ 80 mW 1550 nm distributed feedback laser

(DFB, EM4, Inc.) the output of which is modulated via a low-biased Mach-Zehnder modulator (MZM, JDS Uniphase). The MZM is driven with the output of a 1-GHz step recovery diode (SRD) which produces ~ 54 ps (fullwidth-at-half-maximum, FWHM) voltage pulses with a peak amplitude of $\sim$5.15 V – the normalized drive waveform is shown by the red curve in Figure 3. The resulting optical pulse train [the shape of a single pulse calculated from the SRD output waveform and optical transmission function of the low-biased MZM is shown by the black curve in Fig. 3] is amplified with a commercial erbium-doped fiber amplifier (EDFA, JDS Uniphase OA 400) and appropriately polarized with a fiber polarizartion controller. The RF input signal is impressed onto the pulsed optical carrier by a quadrature-biased dual-output MZM (EOSpace, Inc., $V_\pi \sim 5$ V at 1 GHz). The RF signal is recovered from each arm by direct-detection of the modulated optical intensity using $\sim$ 20 GHz bandwidth photodiodes (Discovery Semiconductor DSC 30S). The photodiode outputs are low-pass filtered ($f_{\text{cutoff}} \approx 470$ MHz) and differenced using a 180° hybrid coupler. The output of the hybrid coupler is filtered once more ($f_{\text{cutoff}} \approx 470$ MHz) to obtain the final RF output of the system.

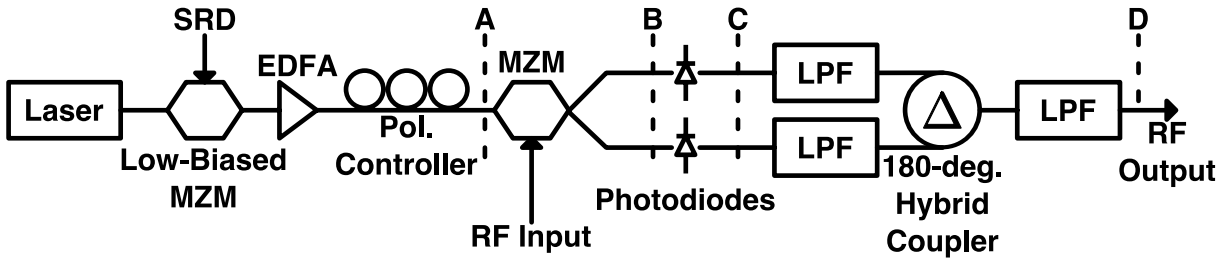

Fig. 2: 1-GHz sampled optical link. SRD: Step-recovery diode, MZM: Mach-Zehnder modulator, LPF: low-pass filter

From the link output power as given in (13) we see that the continuous frequency line is folded into the first Nyquist band. To illustrate this folding operation, single tones at frequencies of f_{o} = 300, 700, 1300, 1700 MHz are injected into the sampled link (the input RF power is nominally $P_{\text{in}} = 0$ dBm). Given the 1 GHz sample rate, all tones are aliased to a frequency of $f = 300$ MHz. Figure 4 illustrates this folding operation for the first four Nyquist bands; the input spectra are shown in black and the spectra of the down-converted signals are shown in red (peak signal amplitude is approximately -16 dBm, the gain of the link is discussed further below). Clearly, the input signals all appear at the alias frequency of 300 MHz. We note, the direction of increasing frequency within the first Nyquist band (after aliasing) depends on whether the input signal originates in an even or odd Nyquist band. As shown by the arrows in Fig. 4 frequency increases from left-to-right for signals falling within an odd Nyquist band. For signals lying in even bands, increasing frequency moves from right-to-left. This behavior provides one step in the eventual disambiguation process and may be exploited by dithering the sampling frequency. The shift in aliased frequency as the sampling rate is changed will allow one to discern whether the signal of interest originates in an even- or odd-Nyquist band. The double-peaked nature of several of the input spectra is simply due to coarse spectral sampling on the spectrum analyzer and frequency instability of the input source. The small feature near 100 MHz is largely due to second-harmonic distortion present in the input signal. The genesis of the other minor spectral features is under investigation.

Radio-Frequency Performance of the Down-Converting Link

For demonstration purposes, the link is configured to operate with an average photocurrent of $I_{\text{avg}} = 10$ mA per photodiode. For this current level and a modulator halfwave voltage of $V_\pi = 5$ V, the gain for a single-photodiode link employing a photodiode with an internal 50 Ω matching resistor is $G = -16.72$

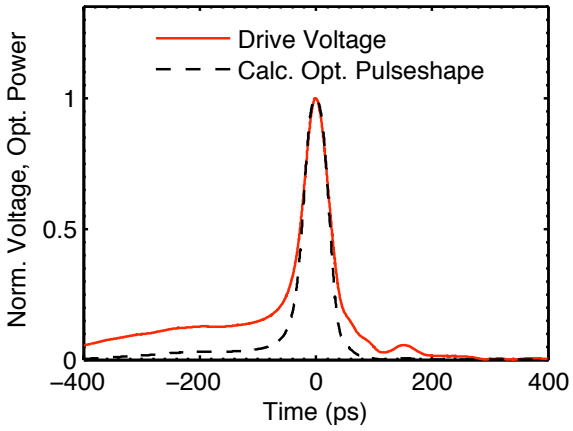

Fig. 3: Normalized time-domain magnitude of the 1-GHz step-recovery diode voltage (red). Optical intensity envelope calculated from the SRD pulse shape and transfer function of the low-biased MZM (black).

dB [one-quarter of that predicted by (15) as determined by maximum power transfer to a matched load). For the balanced configuration the theoretical gain increases to $G = -13.72$ dB (accounting for twice the photocurrent and the ideal 3-dB insertion loss of the hybrid coupler). The measured link gain is shown in Figure 5 (a). For comparison purposes the RF gain of one arm of the balanced link (utilizing a continuous-wave laser source) is measured and subsequently used to calculate the gain of an ideal balanced link (that is, where the hybrid coupler exhibits no excess loss and no phase errors). The calculated gain for the balanced link is shown by the black curve in Fig. 5 (a). The measured single-photodiode gain for frequencies below 1 GHz is approximately $G = -16$ dB (which shows excellent agreement with theory) giving an ideal balanced link gain of $G = -13$ dB. The gain of the down-converting link is determined by tuning the input frequency over the range of 0.25–9.75 GHz in 0.25 GHz steps and measuring link output power at the down-converted frequency of 0.25 GHz (in the first Nyquist band) using a calibrated electronic spectrum analyzer. The measured down-converting link gain is shown by the red circles in Fig. 5 (a) (note, each circle corresponds to the mid-band gain of each Nyquist band ranging from n =1–20). In the first Nyquist band, the gain is measured to be $G = -16.8$ dB. Given the excess loss of the hybrid coupler and RF cabling is approximately 3 dB [which is not accounted for in the ideal link gain shown by the black curve in Fig. 5 (a)], the measured gain shows excellent agreement with that predicted by theory.

The gain of the down-converting link clearly falls off much more rapidly than the frequency-response of the link components (MZM and photodiode, in particular) would dictate. As has been shown in the photonic ADC community, in photonically-sampled systems the bandwidth of the sampling pulse impacts the down-converting system gain [14]. This is readily seen by considering the gain expression given by (15). The quantity $\left|P_n/P_{\text{avg}}\right|^2$ represents the magnitude-squared of the normalized spectrum of the pulse intensity, sampled at the frequency $f = nf_{\text{rep}}$. To show the impact of finite pulse width, the residual gain variation of the down-converting link (after the measured gain is normalized to the gain of a conventional analog link operating at the same photocurrent) is plotted along with the calculated pulse spectrum [magnitude-squared of the Fourier transform of the optical intensity envelope (black curve) in Fig. 3]. Here, we see the rolloff in the pulse spectrum describes the measured gain variation quite well. The small (~ 1 dB) deviation arises from the non-uniformity of the measured gain of the conventional link [black curve in Fig. 5 (a)] which was used to normalized the sampled link gain.

It is important to note that the fundamental folding operation occurs in the optical domain. Therefore,

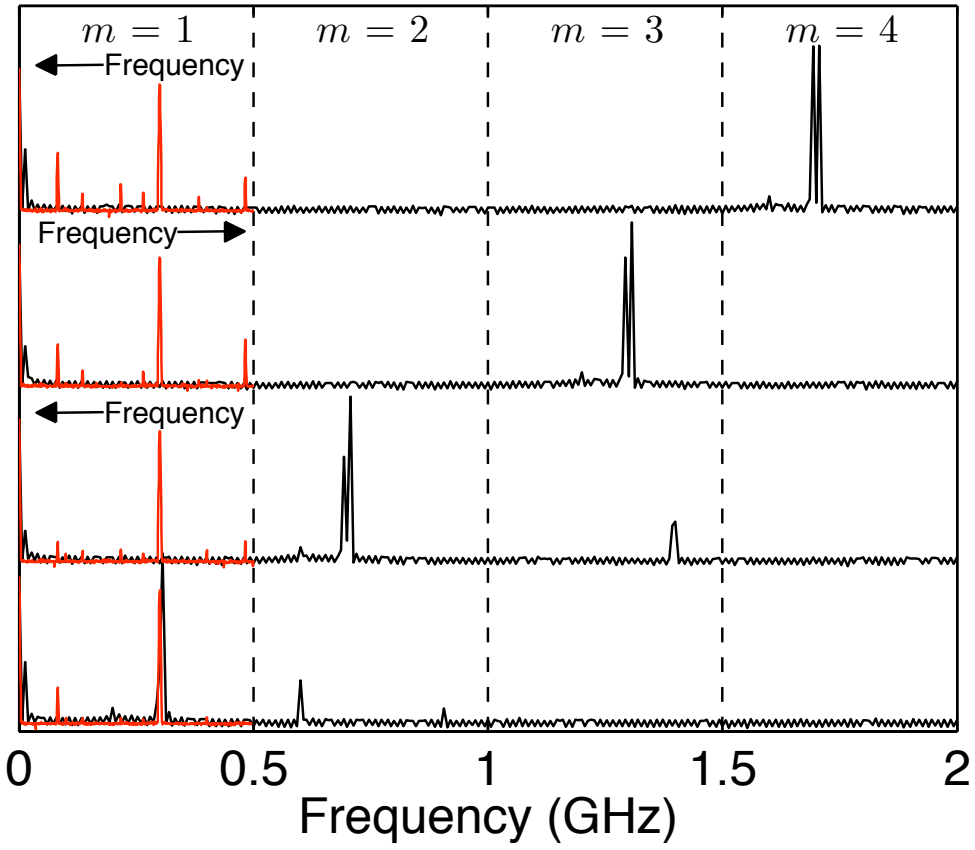

Fig. 4: Measured RF spectra illustrating spectral folding for the first four Nyquist bands. The fundamental frequencies (spectra shown in black) are chosen to be f_o = 300, 700, 1300, 1700 MHz such that all are aliased into the first band at an apparent frequency of 300 MHz (aliased spectra shown in red).

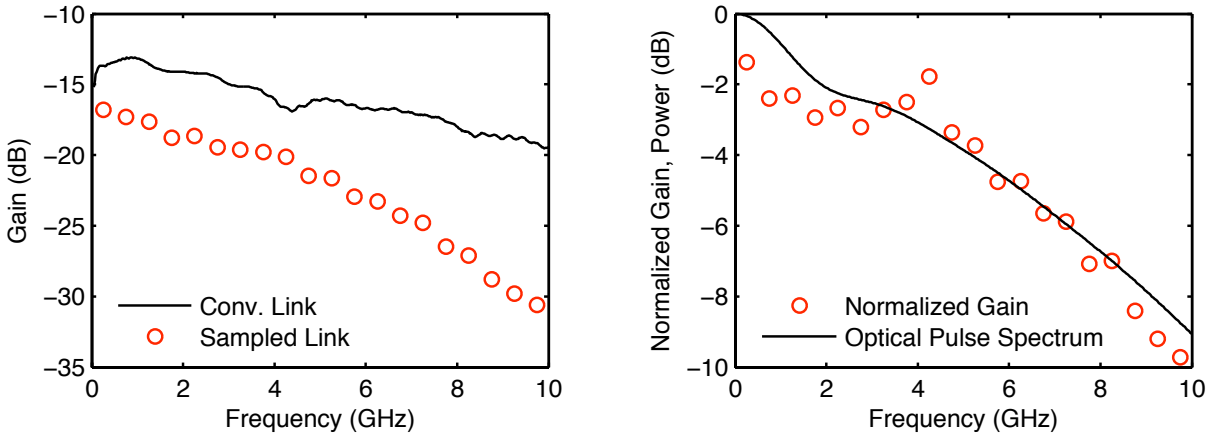

(a) (b)

Fig. 5: (a) Measured RF gain for an average photocurrent of $I_{\text{avg}} = 10$ mA per photodiode. The black curve shows the gain of an ideal balanced link (calculated from the measured RF gain for a single arm, utilizing a CW laser source). The red circles show the measured gain for the 1-GHz sampled link (that is, in a down-conversion mode). (b) Residual gain roll-off due to the shape of the optical sampling pulse. The red circles show the residual gain variation after the gain is normalized to that of the CW link operating with average current $I_{\text{avg}} = 10$ mA [black curve in Fig. 5 (a)]. The black curve shows the pulse power spectrum [calculated Fourier transform of the optical intensity envelope (black curve) in Fig. 3].

in contrast to a conventional analog link, the photodiode bandwidth for the down-converting sampled link need only extend to one-half the sampling frequency – regardless of the highest frequency of interest. This implies that either low-bandwidth photodiodes may be used or that higher pulse energies may be utilized without compromising the link performance. To illustrate this point, the measured current pulse (red) is shown in Figure 6 (a) along with the calculated pulse intensity (black, repeated from Fig. 3). If the photodiode is operating in a purely linear regime, the optical intensity and measured photocurrent should show a one-to-one correspondence (so long as the optical pulse duration significantly exceeds that of the photodiode impulse response). Comparison of the optical intensity to the measured photocurrent clearly shows the effects of transit-time broadening due to high pulse energy [15]. In the frequency-domain, temporal broadening translates to a decrease in bandwidth. In Figure 6 (b) the measured photocurrent spectrum (red) is normalized to the magnitude-squared of the pulse spectrum [black curve, Fourier transform of the black curve in Fig. 6 (a)] . Clearly, the photodiode response bandwidth is significantly narrower than that of the optical pulse (~ 15 dB power difference at 10 GHz). This decrease in bandwidth is, however, not manifested in the measured link gain [the rolloff is well described by the pulse optical bandwidth as shown in Fig. 5 (b)]. In the first Nyquist band ($f < 0.5$ GHz) we see there is only a small amount of compression (< 1 dB) as shown in the inset of Fig. 5 (b). This clearly demonstrates that the required photodiode bandwidth is determined by the high-frequency limit of the first Nyquist band, that is one-half of the sample rate. This means that photodiodes with bandwidths significantly lower than the highest frequency of interest may be utilized for the down-converter. In addition, higher average photocurrents (pulse energies) than allowed in a typical (i.e., non-down-converting) sampled link may be utilized so long as transit-time broadening does not decrease the photodiode bandwidth to less than one-half the sample rate.

The noise sources contributing to the noise power spectral density (PSD) of the sampled link are identical

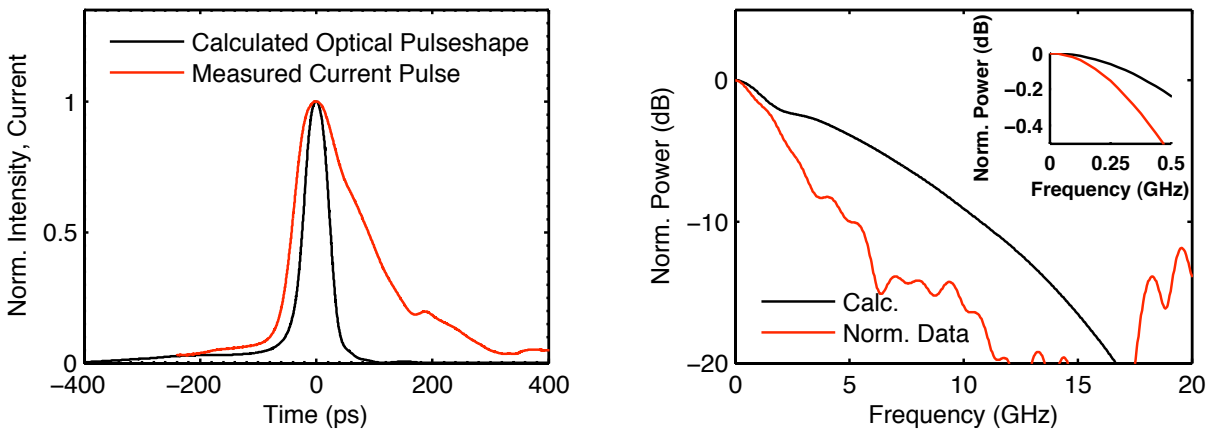

(a) (b)

Fig. 6: (a) Effects of transit-time broadening in the time-domain. The black curve is the calculated optical pulse shape [repeated from Fig. 3 (a)] and the red curves shows the measured current pulse. (b) Calculated Fourier transforms of the time-domain data in (a). Here, the red curve shows the measured current pulse normalized to the calculated spectrum of the optical pulse (black). The inset shows mild compression (~ 1 dB maximum) in the first Nyquist band.

to those in a conventional analog link, namely input and output thermal noise, shot noise, and additional noise arising from the presence of an optical amplifier (here, an EDFA). The total output noise PSD may then be written as

$$N_{\text{tot}} = kT\,(G+1) + N_{\text{sh}}\,(1+\Delta)\,, \tag{19}$$

where the shot noise PSD is expressed in terms of the average photocurrent as

$$N_{\text{sh}} = \frac{1}{4} \times 2qI_{\text{avg}}R_{\text{o}}, \tag{20}$$

q is the magnitude of the electronic charge and ΔN_{sh} represents the additional noise contributed by the presence of an EDFA. The factor of 1/4 appearing above accounts for an internal matching resistor in our photodiodes (maximum power transfer). In the present link, the shot noise PSD [calculated from (20)] is approximately $N_{\text{sh}} = -164$ dBm/Hz – an order of magnitude larger than that due to thermal noise $N_{\text{th}} \approx -174$ dBm/Hz. Because the link gain is much less than unity [see Fig. 5 (a)], the output noise PSD may then be approximated for calculation purposes as being due solely to shot noise and the additional noise arising from the EDFA, that is

$$N_{\text{out}} = N_{\text{sh}}\,(1+\Delta)\,. \tag{21}$$

It should be noted that this operational regime (an approximately shot noise-limited link) the effects of noise aliasing [16] do not affect the system noise figure as they do in electrically-subsampled systems.

The measured noise PSD for the link operating at an average per-diode photocurrent of $I_{\text{avg}} = 10$ mA is shown in Figure 7 (a). Here, the noise is shown for both a conventional link (CW laser, in blue) as well as the sampled link (red). For comparison, the shot noise level of $N_{\text{sh}} = -164$ is shown by the dashed black line. We see there is a small noise penalty [$10\log\,(1+\Delta)$ $\sim$1 dB] [12] arising from the amplified spontaneous emission noise added by the EDFA [17]. Note, the noise contribution of the EDFA is largely suppressed via

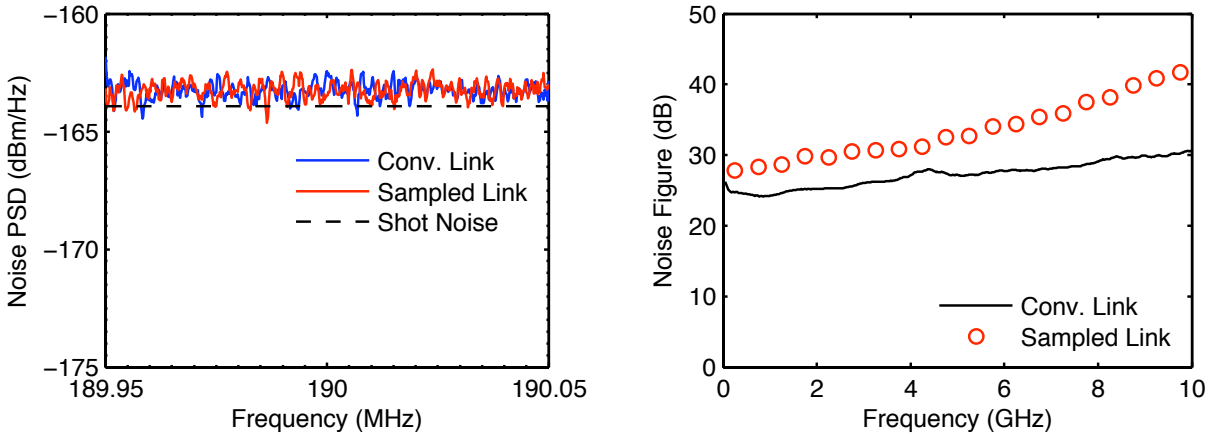

Fig. 7: (a) Measured noise power spectral density for the sampled link (red) and conventional link (blue) for an average photocurrent of $I_{\text{avg}} = 10$ mA per photodiode. For comparison, the theoretical shot noise level is shown by the dashed black line. (b) Noise figure for the sampled- (red circles) and ideal balanced link (black line).

balanced detection (on the order of 20 dB); the penalty here is likely due to a small amplitude imbalance in the two arms of the link.

Using the measured output noise PSD and the measured gain [Fig. 5 (a)] we calculate the link noise figure using (17). The noise figures for the sampled link and the ideal balanced link are shown in Fig. 7 (b) by the red circles and black line, respectively. Here we see generally good agreement with theory; the deviation in measured noise figure below 1 GHz is again due to excess loss in the link (which is not modeled in the gain calculation of the ideal link). At higher frequencies, the increase in noise figure is due to gain rolloff arising from the finite duration of the optical sampling pulse (see Fig. 5 and associated discussion).

As noted previously, nonlinearity of the link is dominated by the third-order distortion of the MZM, so long as the photodiodes operate in a linear regime. Either a true two-tone test of the intermodulation distortion – or a single-tone measurement of harmonic distortion – may be performed to characterize the link linearity in this case. Here, we opt for a simple measurement of harmonic distortion from which we infer the two-tone output third-order intercept point [the harmonic intercept is a factor of 3-times higher (~ 4.8 dB) than that for intermodulation distortion, see for example [18]].

To show the nonlinearity of the link is well-described by conventional analog link theory even in the down-converting operational mode, we perform the harmonic distortion measurement in the first Nyquist band (at a fundamental frequency of 60 MHz) and then repeat the measurement in the second Nyquist band (fundamental frequency of 900 MHz). The measured fundamental and third-harmonic distortion powers are shown versus the input power to the link in Figure 8. Here, data for the first band are shown in red and those for the second band are shown in blue. For both data sets the symbols show the measured data and the solid lines are linear fits to the log-scale data. In the balanced configuration (2-element photodiode array) [19] employing impedance-matched photodiodes and an average per-diode photocurrent of $I_{\text{avg}} = 10.0$ mA, the calculated output third-order intercept point due to intermodulation distortion is approximately $\text{OIP}_3 = 10$ dBm. From the fit data, the measured output third-harmonic intercept points are $\text{OIP}_{3,H} \sim 11$ dBm and $\text{OIP}_{3,H} \sim 11.5$ dBm for the first and second Nyquist bands, respectively. These correspond to third-order

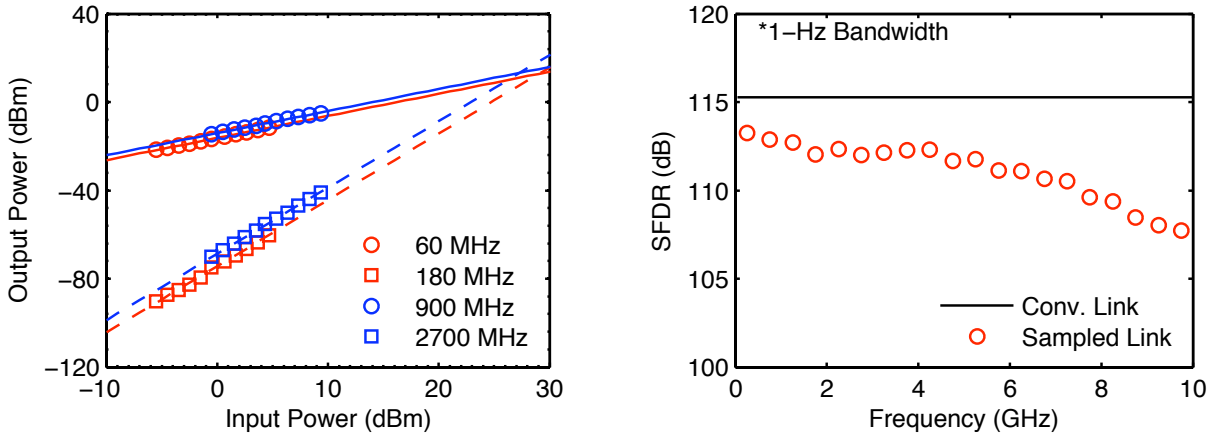

(a) (b)

Fig. 8: (a) Measured fundamental (circles) and third-order harmonic (squares) distortion power in the sampled link. Data measured in the first Nyquist band (0–500 MHz, fundamental frequency $f_o = 60$ MHz, no aliasing) is shown in red and data from the second Nyquist band is shown in blue (500–1000 MHz, the fundamental frequency 900 MHz is aliased into the first band at a frequency of 100 MHz). (b) Spurious-free dynamic range of the sampled- (red circles) and ideal balanced link (black line).

intermodulation distortion levels described by output intercept points of $\text{OIP}_{3,H} \sim 6.2$ and $\text{OIP}_3 \sim 6.7$. Considering the excess loss due to the hybrid coupler and cabling is on the order of 3 dB and the photodiode is slightly compressed [see Fig. 6 (b)], the measured values agree quite well with those predicted by theory.

To illustrate the link dynamic range, we calculate the input third-order intercept point (for intermodulation distortion) as expressed in (16) and use the measured gain and output noise PSD to calculate the spur-free dynamic range according to (18). The SFDR for the sampled link (red circles) and for the ideal balanced link (black line) are shown in Figure 8. We see that the gain of the sampled link compares well with that predicted by theory, with the deviation readily explaind by excess loss and the finite duration of the sampling pulse.

V SUMMARY AND FUTURE DIRECTIONS

In this work we present the first analog description of radio-frequency down-conversion via sampled photonic links. An experimental demonstration of down-conversion across the 1–10 GHz band using a 1-GHz sampled link was used to verify our analysis. This work illustrates that reduced optical pulsewidths are required to extend the down-converter bandwidth. Additionally, we show that only modest photodiode bandwidths are required to achieve down conversion across a wide range of radio frequencies, which substantially reduces the cost of the sampled link architecture. Looking to advance down-converter performance, future work will emphasize the use of modelocked lasers to achieve picosecond (or 100s of femtoseconds) pulsewidths and increased link bandwidth. The use of photodiode arrays will also be pursued to increase the link gain and dynamic range.

VI REFERENCES

[1] G. C. Valley, "Photonic analog-to-digital converters," *Opt. Express*, vol. 15, no. 5, pp. 1955–1982, Mar. 2007.

[2] A. J. Seeds and K. J. Williams, "Microwave photonics," *IEEE J. Lightwave Technol.*, vol. 24, no. 12, pp. 4628–4641, December 2006.

[3] A. E. Siegman and D. J. Kuizenga, "Proposed method for measuring picosecond pulsewidths and pulse shapes in cw mode-locked lasers," *IEEE J. Quantum Electron.*, vol. 6, no. 4, pp. 212–215, Apr. 1970.

[4] D. H. Auston, "Picosecond optoelectronic switching and gating in silicon," *Appl. Phys. Lett.*, vol. 28, no. 3, pp. 101–103, Feb. 1975.

[5] H. F. Taylor, "An optical analog-to-digital converter – design and analysis," *IEEE J. Quantum Electron.*, vol. 15, no. 4, pp. 210–216, Apr. 1979.

[6] R. A. Becker, C. E. Woodward, F. J. Leonberger, and R. C. Williamson, "Wide-band electrooptic guided-wave analog-to-digital converters," *Proc. IEEE*, vol. 72, pp. 808–818, July 1984.

[7] J. A. Bell, M. C. Hamilton, and D. A. Leep, "Optical sampling and demultiplexing applied to A/D conversion," *Devices for Optical Processing*, vol. 1562, pp. 276–280, 1991.

[8] J. A. Bell, M. C. Hamilton, D. A. Leep, H. F. Taylor, and Y. Lee, "Aid conversion of microwave signals using a hybrid optical/electronic technique," *Optical Technology for Microwave Applications V*, vol. 1476, pp. 326–329, 1991.

[9] P. W. Juodawlkis, J. C. Twichell, G. E. Betts, J. J. Hargreaves, R. D. Younger, J. L. Wasserman, F. J. O'Donnell, K. G. Ray, and R. C. Williamson, "Optically sampled analog-to-digital converters," *IEEE Trans. Microwave Theory Tech.*, vol. 49, no. 10, pp. 1840–1853, Oct. 2001.

[10] J. Kim, M. J. Park, M. H. Perrott, and F. X. Kärtner, "Photonic subsampling analog-to-digital conversion of microwave signals at 40-GHz with higher than 7-ENOB resolution," *Opt. Express*, vol. 16, no. 21, p. 1650916515, Oct. 2008.

[11] J. D. McKinney and K. J. Williams, "Sampled analog optical links," *IEEE Trans. Microwave Theory Tech.*, vol. 57, no. 8, pp. 2093–2099, Aug. 2009.

[12] V. J. Urick, M. S. Rogge, F. Bucholtz, and K. J. Williams, "The performance of analog photonic links employing highly compressed erbium-doped fiber amplifiers," *IEEE Trans. Microwave Theory Tech.*, vol. 54, no. 7, pp. 3141–3145, July 2006.

[13] C. H. Cox III, *Analog Optical Links: Theory and Practice*. New York: Cambridge University Press, 2004.

[14] P. W. Juodawlkis, J. J. Hargreaves, R. D. Younger, G. W. Titi, and J. C. Twichell, "Optical downsampling of wide-band microwave signals," *IEEE J. Lightwave Technol.*, vol. 21, no. 12, pp. 3116–3124, Dec. 2003.

[15] P.-L. Liu, K. J. Williams, M. Y. Frankel, and R. D. Esman, "Saturation characteristics of fast photodetectors," *IEEE Trans. Microwave Theory Tech.*, vol. 47, no. 7, pp. 1297–1303, July 1999.

[16] R. G. Vaughn, N. L. Scott, and D. R. White, "The theory of bandpass sampling," *IEEE Trans. Signal Processing*, vol. 39, no. 9, pp. 1973–1984, Sept. 1991.

[17] E. Desurvire, *Erbium-Doped Fiber Amplifiers: Principles and Applications*. New York: John Wiley and Sons, Inc., 1994.

[18] D. M. Pozar, *Microwave Engineering*, 3rd ed. Hoboken: John Wiley and Sons, Inc., 2005.

[19] V. J. Urick, A. S. Hastings, J. D. McKinney, C. Sunderman, J. F. Diehl, P. S. Devgan, K. Colladay, and K. J. Williams, "Photodiode linearity requirements for radio-frequency photonics and demonstration of increased performance using photodiode arrays," in *IEEE International Topical Meeting on Microwave Photonics*, vol. 1, Gold Coast, Australia, Oct. 2008, pp. 86–89.